# Probing interlayer interactions and commensurate-incommensurate transition in twisted bilayer graphene through Raman spectroscopy

Vineet Pandey,<sup>†</sup> Subhendu Mishra,<sup>‡</sup> Nikhilesh Maity,<sup>‡</sup> Sourav Paul,<sup>†</sup> Abhijith M B,<sup>†</sup> Ajit Roy,<sup>¶</sup> Nicholas R Glavin,<sup>¶</sup> Kenji Watanabe,<sup>§</sup> Takashi Taniguchi,<sup>∥</sup> Abhishek Kumar Singh,<sup>\*,‡</sup> and Vidya Kochat<sup>\*,†</sup>

†Materials Science Centre, Indian Institute of Technology, Kharagpur, West Bengal - 721302,India

‡Materials Research Centre, Indian Institute of Science, Bengaluru - 560012, India
¶Air Force Research Laboratory, Wright-Patterson Air Force Base, OH - 45433, United States
§Research Center for Electronic and Optical Materials, National Institute for Materials Science,

1-1 Namiki, Tsukuba 305-0044, Japan

||Research Center for Materials Nanoarchitectonics, National Institute for Materials Science, 1-1
Namiki, Tsukuba 305-0044, Japan

E-mail: abhishek@iisc.ac.in; vidya@matsc.iitkgp.ac.in

### **Abstract**

Twisted 2D layered materials have garnered a lot of attention recently as a class of 2D materials whose interlayer interactions and electronic properties are dictated by the relative rotation / twist angle between the adjacent layers. In this work, we explore a prototype of such

a twisted 2D system, artificially stacked twisted bilayer graphene (TBLG), where we probe the changes in the interlayer interactions and electron-phonon scattering pathways as the twist angle is varied from 0 to 30°, using Raman spectroscopy. The long range Moiré potential of the superlattice gives rise to additional intravalley and intervalley scattering of the electrons in TBLG which have been investigated through their Raman signatures. The density functional theory (DFT) calculations of the electronic band structure of the TBLG superlattices was found to be in agreement with the resonant Raman excitations across the van Hove singularities in the valence and conduction bands predicted for TBLG due to hybridization of bands from the two layers. We also observe that the relative rotation between the graphene layers has a marked influence on the second order overtone and combination Raman modes signalling a commensurate-incommensurate transition in TBLG as the twist angle increases. This serves as a convenient and rapid characterization tool to determine the degree of commensurability in TBLG systems.

**Keywords:** twisted bilayer graphene, Raman spectroscopy, combination modes, density functional theory, commensurate-incommensurate transition

2D layered materials with twist dependent stacking have been a hot topic of research recently, as the electronic properties of such systems critically depend on the superlattice formation due to relative rotation between the layers. A prototype system, twisted bilayer graphene (TBLG) has been a typical example of the superlattice-induced modified bandstructure with several new phases such as correlated insulator, superconductivity and ferromagnetism emerging at critical twist angles called the magic angles. <sup>1-4</sup> In a TBLG Moiré superlattice, alternating AA and AB stacked regions emerge, leading to a hexagonal superlattice potential which folds the bands into a mini Brillouin zone. The adjacent Dirac cones in this mini Brillouin zone hybridize leading to bands with reduced Fermi velocity near charge neutrality point, furthermore developing into flat bands for the critical angles close to 1.1° or the magic angles. <sup>5</sup> For small values of twist angles, the atoms adjust with the superlattice landscape forming an energetically favourable commensurate system, by gaining van der Waals energy, but at the expense of elastic energy. As the Moiré period becomes smaller, the van der Waals energy gain over the elastic energy loss is no longer

compensated, leading to an incommensurate system of bilayers, where each layer is independent of the other. <sup>6</sup> This shows that the mechanical and electronic degrees of freedom are closely related in TBLG systems, wherein the twist angle determines the modifications to the bandstructure and also the interlayer coupling.

The 2D quantum materials-based technology projections are focussed on identifying artificially stacked 2D heterostructures with combined and novel functionalities of various 2D materials. In this context, it becomes very important to understand how this unique degree of freedom of twisting layers determines the fundamental properties such as mechanical coupling, elasticity, electronic band structure and electron-phonon coupling in such 2D heterostructure stacks. In this work, we have investigated these properties in twisted graphene bilayers, which is a very promising system of homobilayers exhibiting a rich variation of the electronic properties with changing relative rotation between the layers. While at low angles, emergent phases attributed to flat bands have been observed, at high angles close to 30°, TBLG forms an incommensurate superlattice with quasicrystalline order and mirrored Dirac cones originating from strong interlayer interaction. <sup>7–9</sup> A significant experimental effort has gone into studies of the Moiré superlattices in TBLG concentrating on STM and ARPES. <sup>10–20</sup> We have studied the effect of the Moiré potential on the interlayer coupling and bandstructure by using Raman spectroscopy, which is a well-established powerful characterization technique to investigate the layer numbers, disorder and stacking orientations in bi and tri-layer graphene systems. <sup>21–26</sup> Raman studies on folded graphene and chemical vapor deposition (CVD) grown rotationally stacked bilayer graphene showed emergence of new modes due to the intravalley and intervalley scattering of electrons by Moiré potential. 27-36 Also it was found that Raman studies as a function of laser energy and twist angle can trace the positions of the van Hove singularities (vHs) in the conduction and valence bands of TBLG originating from the hybridization of the Dirac cones of the twisted graphene layers. <sup>37–39</sup> Modifications of the electronic band structure and the phonon dispersion in TBLG was suggested to give rise to frequency shifts of the 2D peak and well as the lineshape and width. 40-45 On the other hand, the Raman studies in artificially stacked bilayer graphene systems has been very limited. Similar observations were noted in

twisted CVD bilayers fabricated by PMMA-assisted tansfer, while in artificially stacked exfoliated bilayer graphene, studies reported the variations in in-plane anisotropy and superlattice-induced transverse acoustic Raman modes with the mis-orientation angle. <sup>46,47</sup> For TBLG close to magic angles, the G and 2D bands were significantly influenced by the electron-phonon interactions and the areal coverage of AB and BA stacked regions separated by strain soliton regions. <sup>48</sup>

In this work, we have studied the electron-phonon scattering mechanisms in artificially stacked TBLG in detail and substantiated our results with that of folded and CVD grown graphene Raman signatures. The various intravalley and intervalley scattering mechanisms induced by Moiré potential have been investigated and the results have been explained by variations in the electronic bandstructure and density of states (DOS) obtained from density functional theory (DFT) calculations. In addition we observe that the resonance arising from the transition between the vHs in the valence and conduction band also presents interesting features in G and M bands. Our work shows that the tunability of the vHs in rotationally misoriented bilayer graphene can give rise to enhanced absorption leading to wavelength selective photodetectors in future. Finally we also explore the overtone and combination modes in TBLG which serves as a definitive signature of commensurate to incommensurate transition at higher twist angles and mechanical decoupling of the layers.

# **Results and discussion**

The TBLG samples were fabricated using the tear and stack method using a 2D transfer system (from CryoNano Labs) for various twist angles as shown in the optical micrographs in top panels of Fig. 1a-d. <sup>49</sup> The middle panel shows the superlattice evolution for the corresponding angles from which it is evident that at low angles (< 12.5°) a long-range Moiré pattern evolves and the TBLG can be approximately treated as a system with Moiré period governed translational symmetry. At larger twist angles (> 20°), the Moiré period is in the order of atomic length scale evolving to a quasi-crystalline (QC) state at twist angles of 30°. The FFT of these TBLG systems gives a direct estimation of the Moiré wavevector, **q**, whose magnitude is plotted in Fig. 1e. The QC TBLG

lattice which lacks translational symmetry shows a 12-fold rotational order in the FFT analysis. A geometrical analysis in the reciprocal space reveals that the additional periodicity due to the Moiré potential results in a new mini-Brillouin zone with a twist angle ( $\theta$ ) dependent lattice vector which is the resultant of the wavevectors  $\mathbf{q}_1$  and  $\mathbf{q}_2$  corresponding to the top and bottom layers and is given by

$$q(\theta) = \frac{8\pi}{\sqrt{3}a} \sin\left(\frac{\theta}{2}\right) \tag{1}$$

where a = 0.246 nm is the lattice parameter of graphene.<sup>29</sup> The values obtained for  $q(\theta)$  from this calculation perfectly matches the values obtained directly from the FFT analysis as can be seen from Fig. 1e.

The TBLG samples were studied through Raman spectroscopy using 532 nm excitation and the spectra corresponding to the twist angles  $8^{\circ}$ ,  $10^{\circ}$ ,  $12.5^{\circ}$ ,  $20^{\circ}$  and  $30^{\circ}$  are shown in Fig. 2a,b along with a single layer graphene (SLG) and Bernal-stacked bilayer graphene (BLG). The Gpeak arising from the doubly degenerate zone center  $E_{2g}$  mode occurs at 1582 cm<sup>-1</sup> and shows negligible frequency shift with the twist angle. Interestingly at twist angle of  $12.5^{\circ}$ , we observe a huge enhancement of the G-peak intensity. Such an enhancement has been reported earlier in CVD grown bilayer graphene samples at misorientation angles of  $10^{\circ}$  to  $12^{\circ}$  under 633 nm and 532 nm excitation.  $^{30,39,41}$  This has been attributed to the resonant condition when the laser excitation energy matches the parallel band singularity in TBLG. Here there are a large number of states with the same energy difference, giving rise to Raman scattering paths with identical phases that interfere constructively and result in considerable enhancement of G-peak.  $^{38,45}$  When the Dirac cones of the top and bottom layers overlap, the DOS is modified due to the interactions leading to hybridization gap and vHs emerge in the conduction and valence bands of TBLG. When the excitation laser energy  $E_L$  matches this energy separation between the conduction and valence band vHs, which in turn is dependent on the twist angle  $\theta$ , resonance occurs as per the condition

$$\theta_C = \frac{3aE_L}{\hbar v_f 4\pi} \tag{2}$$

where  $v_f$  is the Fermi velocity in SLG (10<sup>6</sup> m/s) and  $\theta_C$  is the critical twist angle. For excitation wavelength of 532 nm (2.33 eV),  $\theta_C \sim 12.3^{\circ}$  which matches well with the twist angle where the resonance is observed experimentally. This is also the first observation of G-peak resonance in TBLG fabricated by tear and stack method. In the Raman map in Fig. 2c (given in red, bottom panel), the G-peak resonance is clearly observable in the TBLG region, whereas the region of SLG has much lower intensity. We show later that this picture of parallel bands is in accordance with the band structure obtained from DFT simulations as well.

As opposed to the G-peak, the 2D peak shows significant variations in frequency and intensity as a function of twist angle. At twist angles larger than 10°, we observe a notable blue shift in our TBLG samples. Previous studies have attributed this blue shift to reduction in Fermi velocity in TBLG. <sup>39,40</sup> The maximum blue shift occurs at  $\theta_C$  and decreases at lower and higher twist angles as seen in the plot in Fig. 2e. But theoretical calculations show that significant reduction in Fermi velocity happens for twist angles  $< 5^{\circ}$ , contrary to our observations. <sup>50–52</sup> The possible origin of the 2D peak shift will be discussed later. Another interesting aspect of the 2D peak is the single Lorentzian behaviour at twist angles larger than 8°. This is in contrast with the convoluted peak picture for the Bernal-stacked BLG and TBLG with misorientation angles less than 5° reported earlier. 21,48 It proves that the Dirac nature of the bands from individual layers are retained at higher twist angles. With increase in twist angle, the intensity ratio of the 2D peak to the G peak,  $I_{2D}/I_G$  increases to about 4 times that of SLG, while the FWHM of the single Lorenztian reduces and becomes similar to that of SLG as shown in Fig. 2d. This can be attributed to the differences in the scattering mechanisms as a function of twist angle described in the schematics in Fig. 2b. For  $\theta > \theta_C$ , the separation between the vHs,  $\Delta E_{vHs} > E_L$  and hence the energy dispersion is linear with negligible interaction between the layers. The iTO phonons contribute to the double resonance process of intralayer intervalley scattering between the K and K' valleys of the two layers. Since the frequencies of the scattering phonons, energy dispersion and electron-phonon coupling are all identical for the two layers, the resulting 2D peak should have a higher intensity than SLG and also similar FWHM. At  $\theta = \theta_C$ ,  $\Delta E_{\nu Hs} \approx E_L$ , and a large number of optical transitions occur due to the

vHs which increases the joint DOS. There is also a transition from linear dispersion to a flat band dispersion, due to which the phonons giving rise to intervalley scattering have larger wavevectors which also explains the huge blue shift of the 2D peak at  $\theta_C$ . The flat band and the joint DOS also gives rise to slight variations in the wavevectors of the scattering phonons leading to an increased FWHM. Finally, at  $\theta < \theta_C$ ,  $\Delta E_{vHs} < E_L$ , due to the increased interlayer interactions, along with intralayer scattering, interlayer intervalley scattering is also possible. This gives rise to a complex interference between the scattered phonons reducing the intensity and increasing the FWHM at low twist angles as observed in Fig. 2d. The 2D Raman maps for the various twist angles are shown in Fig. 2c, which clearly indicate that the intensity is uniform throughout the entire TBLG region and also is a good experimental proof for a spatially homogeneous superlattice structure.

At low angles of 8°, we observe an additional peak at 1625 cm<sup>-1</sup>, which is absent for higher twist angles as shown in Fig. 2f. This peak is attributed to the R'-peak which arises due to the intra-valley double resonance process, where the excited electron is elastically scattered by its interaction with the Moiré potential through the rotational wavevector,  $q(\theta)$  to the point in the same valley with equal and opposite momentum. A phonon with a wavevector same as  $q(\theta)$  given by  $Q_{intra}$  is created and scatters the electron back inelastically, which finally combines with a hole to give the Raman shift observed. From the phonon dispersion curve of graphene, we observe that  $Q_{intra}$  corresponds to the LO phonon frequency of 1625 cm<sup>-1</sup> which lies close to the  $\Gamma$  point in the first Brillouin zone along the  $\Gamma$ K direction and has strong electron-phonon coupling. <sup>29,53</sup> For this type of intra-valley scattering for a twist angle of  $\theta$  the incident photon energy is given by

$$E_L^{intra}(\theta) = \hbar v_F q(\theta) \tag{3}$$

For  $E_L^{intra} = 2.33$  eV,  $q(\theta)$  turns out to be 0.365 Å<sup>-1</sup> corresponding to a twist angle of 7.1° from Fig. 1e, which is very close to the experimental twist angle of 8°.

The experimental Raman signatures have also been corroborated by first-principles DFT calculations performed using Vienna ab initio simulation package (VASP). 54,55 The electronic band

structure of SLG has a linear band dispersion in the vicinity of high-symmetry point K and results in four-fold degenerate states from the  $p_z$  orbital of the carbon atom. On the other hand, in TBLG, at energies far from the Fermi level, the bands are modified and spilt, resulting in the appearance of extrema for some of the sub-bands close to the M-point in the Brillouin zone as indicated by 1, 2, 3 and 4 in Fig. 3b. 56 These saddle points near M point in the band structure of TBLG results in twist-induced spikes (singularity 2 and 3) and twist induce kinks (singularity 1 and 4) in DOS known as vHs shown in Fig. 3e. These saddle points/vHs play an important role in determining the optical transitions when light is incident on these systems. These vHs differences ( $\Delta E_{vHs}$ ) give the information of strength and the energy of the transitions. In TBLG, the allowed transitions are from 1-3 and 2-4, while 1-4 and 2-3 transitions are forbidden.<sup>57</sup> The  $\Delta E_{\nu Hs}$  variation with twist angle of TBLG for allowed and forbidden transitions are given in Fig. 3f. From the Fig. 3f, it is observed that the vHs splitting increases with increasing the twist angle of TBLG, which is consistent with the previous literature. <sup>58</sup> When the excitation laser energy  $E_L$  matches the energy separation between the conduction and valence band vHs of allowed transition (transition 1-3 or 2-4), a large number of excitations occur. The calculated allowed transition energies of TBLG for twist angles 9.43°, 13.2°, 21.8°, and 27.8° are 1.46, 1.89, 2.70, and 2.74 eV, respectively. The experimental  $E_L$ is very close to the calculated  $\Delta E_{\nu Hs}$  corresponding to TBLG of twist angle 13.2°. Therefore, our theoretical observation suggests that the closest resonance ( $E_L \approx \Delta E_{\nu Hs}$ ) for laser energy of 2.33 eV occurs at the vicinity of  $\theta = 13.2^{\circ}$ , consistent with our experimental result and  $\theta_C = 12.3^{\circ}$  calculated based on continuum model.<sup>35</sup> Hence, our theoretical study and experimental observation indicate that the resonance of  $E_L$  with  $\Delta E_{\nu Hs}$  is the fundamental reason for the enhancement of the G peak in TBLG of a twist angle of  $12.5^{\circ}$ .

Apart from the first order Raman modes, we also investigated the second order peaks and combination modes which also yield crucial information regarding the layer stacking. Specifically, we have looked into the Raman spectrum in the range of 1700 cm<sup>-1</sup> to 2100 cm<sup>-1</sup> in the TBLG and compared with SLG and Bernal stacked BLG as shown in Fig. 4a. In BLG, a peak is observed at 1750 cm<sup>-1</sup> which is the M band, an overtone of oTO phonon giving rise to an electron double res-

onant intravalley scattering. This mode becomes Raman active due to interlayer coupling. Hence it is absent in SLG, but present in BLG, multilayer graphene and graphite with Bernal stacking. <sup>59</sup> We find that the M-band is absent in TBLG samples clearly indicating deviations from Bernal stacking which renders the oTO phonon Raman inactive. The absence of M band indicates significant weakening of the interlayer interactions as compared to Bernal stacked BLG. Surprisingly, we observe the M-band for twist angle of 12.5°. It has been shown that M-band can selectively be seen in single-walled carbon nanotubes (SW-CNT) of certain chiralities and diameters when the laser excitation energy matches the transition energy between the valence and conduction band vHs. <sup>60,61</sup> On a similar note, the observation of the M-band coinciding with the G-peak resonance enhancement, suggests its origin related to the resonant excitation between vHs and inelastic scattering involving oTO phonons.

We also investigate the reported combination modes around 1860 cm<sup>-1</sup> and 2000 cm<sup>-1</sup> for the TBLG samples. 62,63 These modes are shown for TBLG samples along with SLG and BLG in Fig. 4a. The nomenclature of the various phonons giving rise to these combination modes are given in Table 1. At 1860 cm<sup>-1</sup>, we observe that for the BLG, there are two convoluted peaks corresponding to LO<sup>-</sup>TA (LOTA@ $\Gamma$ ) and LO<sup>-</sup>TO'@ $\Gamma$  which reduces to a single narrow peak attributed to LOTA@ $\Gamma$  in SLG. As the twist angle increases, we observe the reduction in intensity of the peak corresponding to LO<sup>-</sup>TO'@Γ. In BLG, around 2000 cm<sup>-1</sup>, the phonon contributions around the  $\Gamma$  and K points are comparable leading to a band which is a convolution of three peaks corresponding to scattering by the phonon modes LO<sup>+</sup>LA@ $\Gamma$ , LO<sup>-</sup>LO'@ $\Gamma$  and TOZO@K. The peak corresponding to TOZO@K vanishes for the SLG as a result of negligible electron-phonon coupling of ZO<sup>-</sup>@K, while the interlayer interactions restore this mode in BLG.<sup>59</sup> At high twist angles, we observe the absence of the Raman peak from TOZO@K. Altogether, we find that above 12.5° twist angle, the Raman modes in the range of 1700 cm<sup>-1</sup> to 2100 cm<sup>-1</sup> resemble that of SLG. This suggests the transition from a commensurate (C-TBLG) to an incommensurate (I-TBLG) sublattice with increasing rotational misorientation. We also observe a significant blue shift of the phonon modes associated with LOTA and LOLA at higher twist angles when compared to

that of SLG as shown in Fig. 4b. This shows a stiffening of the phonon modes possibly due to a compressive strain in I-TBLG as opposed to the C-TBLG. The blue shift of the combination modes also follow the same variation as that of 2D peak. Such blue shift of the 2D peak has also been observed earlier in h-BN encapsulated graphene with incommensurate superlattice structure. <sup>64</sup> 30° TBLG is considered to be a quasicrystal with no long-range translational symmetry but rotational symmetry being preserved with a dodecagonal pattern of arrangement that can also be inferred from the reciprocal space as shown in Fig. 4d. The evolution from the 6-fold symmetry at 10° to the 12-fold symmetry at 30° is represented in the reciprocal space in Fig. 4d. From the combination modes Raman spectrum and symmetry analysis of the reciprocal space, we conclude that TBLG with twist angle of 20° behaves as incommensurate lattice with no quasicrystalline symmetry.

Table 1: Combination modes between 1860 cm<sup>-1</sup> and 2000 cm<sup>-1</sup> for the TBLG samples

Combination modes	Vibrational Raman modes	Significance
$iLO + iTO \text{ or } iLO^+ + iTO^+$	$E_g$	Doubly degenerate in-plane
		symmetric with in-phase and
		out-of-phase displacement
ZO' and ZO <sup>+</sup>	$A_{1g}$	Non-degenerate out-of-plane
		symmetric with in-phase and
		out-of-phase displacement
ZA and ZO <sup>-</sup>	$A_{2u}$	Non-degenerate out-of-plane
		anti-symmetric with in-phase
		and out-of-phase displace-
		ment
LA + TA and LO <sup>-</sup> + TO <sup>-</sup>	$E_u$	Doubly degenerate in-plane
		anti-symmetric with in-phase
		and out-of-phase displace-
		ment

Even though, the interlayer interactions are weakened in the I-TBLG, it is important to see if there is any contribution of the Moiré potential to the electron scattering mechanisms in the two layers. To study this we have looked for signatures of predicted R-peak arising from the inter-valley double resonant scattering. Here an excited electron is elastically scattering to another inequivalent valley by a large rotation momentum  $q(\theta)$  and then inelastically backscattered to the same k value by a zone boundary phonon  $Q_{inter}$ , followed by recombination with hole giving the Ra-

man scattered photon.  $^{29}$  Near the K-point, the TO phonon branch has very strong electron-phonon coupling and provide the momentum required for the inter-valley scattering. For a twist angles of  $30^{\circ}$  and  $20^{\circ}$ , we observe low intensity peaks at  $\sim 1375~\rm cm^{-1}$  and  $\sim 1435~\rm cm^{-1}$  respectively in the Raman spectrum shown in Fig. 4c which also matches with the predicted values for the R peaks. This shows that even in incommensurate lattices, the Moiré potential can influence the electron scattering mechanisms.

# **Conclusions**

In conclusion, we have carried out detailed Raman spectroscopic investigations of TBLG and find clear Raman signatures which can be correlated with the changes in the electronic bands due to the Moiré potential induced by twisting the graphene layers. When the laser excitation matches the energy separation between the vHs arising from hybridization between the bands of the two layers, resonance features arise in the G-peak and the M-band in TBLG. The Moiré potential can also induce intra- and inter-valley scattering processes giving rise to twist angle specific peaks in the Raman spectrum of TBLG. The observed upshift of the 2D peak and combination modes at high twist angles can be attributed to the compressive strain in incommensurate superlattice. The 2D peak intensity and FWHM, together with the Raman spectrum of the combination modes can jointly distinguish between commensurate and incommensurate superlattices formed in TBLG making this a valuable characterization technique to investigate the degree of commensurability in graphene-based 2D heterostructures.

### Methods

### Raman measurements

Raman scattering measurements were performed using the WITEC alpha300 system equipped with 1800 lines/mm grating. The excitation was done using a 532 nm diode laser with a power of approximately 16.87 mW and a spot size of 500 nm. To observe the samples, a 100x objective lens with a 0.95 NA was utilized and the intensity was detected using a CCD. The data analysis was

carried out using the WITEC Project software.

### **DFT** calculations

In order to gain insights into the changes in the interlayer interactions and electron-phonon scattering of TBLG with twist angle, the first-principles DFT calculations are performed using VASP. 54,55 The all-electron projector augmented wave (PAW) potentials are used to represent the ion-electron interactions in the TBLG systems. 65,66 For the calculations, the electronic exchange and correlation part of the potential is described by the Perdew-Burke-Ernzerhof (PBE) generalized gradient approximation (GGA). 67 A 20 Å vacuum is used along the c-axis in order to avoid spurious interactions between periodically repeated images of single layer and bilayer TBLG systems. The Kohn Sham orbitals are expanded using the plane wave basis sets with an energy cut-off of value 500 eV. All structures are relaxed using the conjugate-gradient algorithm until the Hellmann-Feynman forces on every atom are less than 0.005 eVÅ<sup>-1</sup>. For bilayer graphene and TBLG, the lattice parameters and atomic positions are optimized by considering the weak van der Waals (vdW) interactions between the layers as implemented in Grimme's PBE-D2. 68 For relaxation, a well-converged Monkhorst-Pack (MP) k-grid of 12×12×1 was used to sample the Brillouin zone (BZ) of SLG and BLG. 69 For TBLG of twist angles 27.8° and 21.8°, the k-grid of 8×8×1 is used, and for 13.2° and 9.43° twist angles, a 6×6×1 k-grid is used.

## **FIGURES**

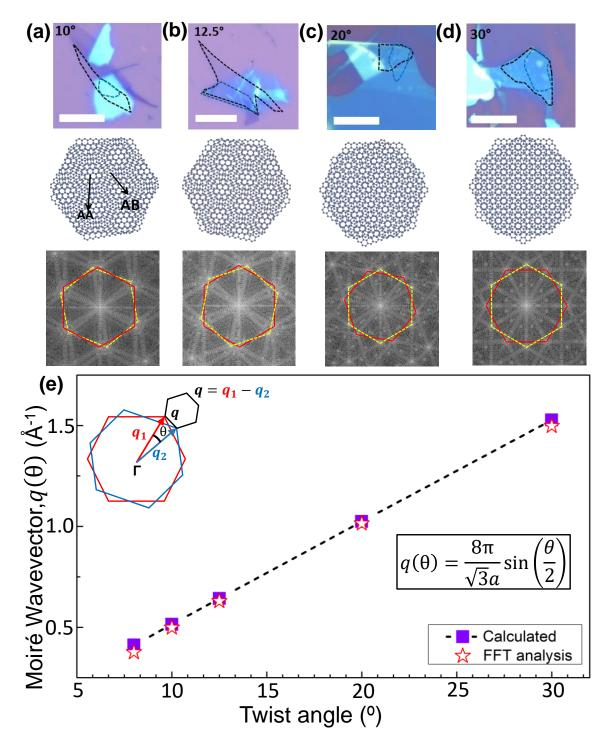


Figure 1: (a) to (d) Optical images of samples (first row)(scale:  $10 \,\mu\text{m}$ ), real space lattice structures (second row) and FFT analysis with reciprocal space representing first Brillouin zone seperation (third row) for  $10^{\circ}$ ,  $12.5^{\circ}$ ,  $20^{\circ}$  and  $30^{\circ}$  TBLG samples. (e) Plot of  $q(\theta)$  vs  $\theta$  for twist angles ranging from  $8^{\circ}$  to  $30^{\circ}$  TBLG samples showing the values calculated by the formula in the inset and obtained from the FFT analysis of Moiré wave-vector  $q(\theta)$  as shown in inset figure.

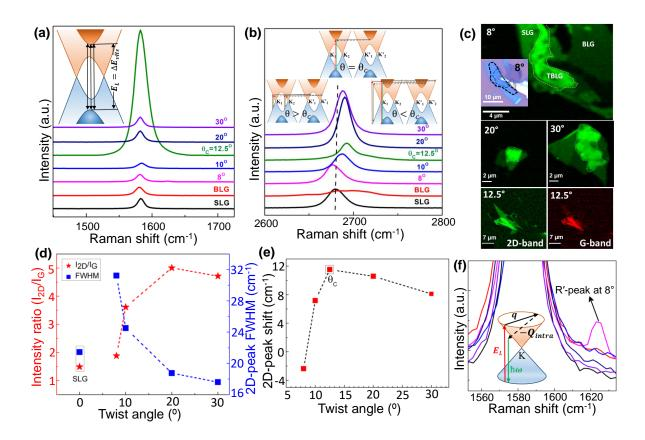


Figure 2: (a) Raman shift of G-peak for all TBLG samples. G-peak enhancement occurs for  $\theta_C = 12.5^{\circ}$  due to parallel band transitions (inset figure) at  $E_L = \Delta E_{vHs}$ . (b) Raman shift of 2D-peak for all TBLG samples. The various intervalley scattering possibilities occuring for  $\theta > \theta_C$ ,  $\theta = \theta_C$  and  $\theta < \theta_C$  are shown in the inset. (c) Raman maps of 2D peak (green) for different TBLG samples. Raman map for the G peak (red) shows a resonance enhancement for the 12.5° TBLG. (d) Plot for  $I_{2D}/I_G$  and 2D-peak FWHM as a function of twist angle,  $\theta$  is shown for different TBLG samples. (e) Plot of 2D-peak shift of TBLG relative to the SLG as a function of twist angle,  $\theta$ . (f) Appearance of R'-peak for 8° TBLG sample along with the intravalley scattering process due to Moiré potential as depicted in the inset.

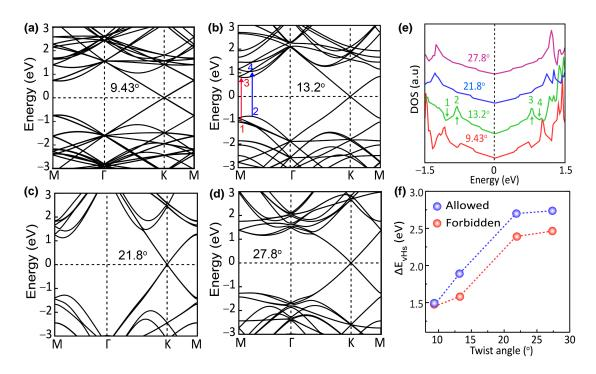


Figure 3: Electronic band structures of TBLG for twist angles of (a)  $9.43^{\circ}$ , (b)  $13.2^{\circ}$ , (c)  $21.8^{\circ}$  and (d)  $27.8^{\circ}$ , respectively. The red and blue arrows in Figure (b) represent the allowed ( $1\rightarrow 3$  or  $2\rightarrow 4$ ) optical transitions. (e) The calculated total DOS of TBLG for twist angles  $9.43^{\circ}$ ,  $13.2^{\circ}$ ,  $21.8^{\circ}$  and  $27.8^{\circ}$ . The allowed ( $1\rightarrow 3$  or  $2\rightarrow 4$ ) is given for  $13.2^{\circ}$ . (f) The value of  $\Delta E_{vHs}$  of allowed ( $1\rightarrow 3$  or  $2\rightarrow 4$ ) and lowest forbidden transitions ( $2\rightarrow 3$ ) in TBLG for twist angles  $9.43^{\circ}$ ,  $13.2^{\circ}$ ,  $21.8^{\circ}$  and  $27.8^{\circ}$  respectively.

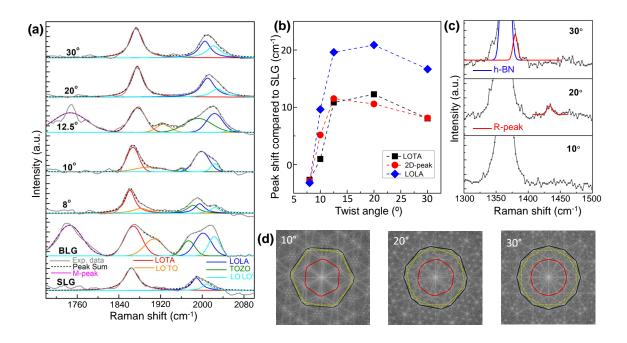


Figure 4: (a) Plot of Raman shift for M-band and combination modes (near  $1860~\text{cm}^{-1}$  and  $2000~\text{cm}^{-1}$ ) in different TBLG samples. Peak-fitting of the data identifies all the possible combination modes. (b) Raman peak shift of TBLG compared to SLG for LOTA , LOLA and 2D peaks for different TBLG samples. (c) R-peak (in red) appears for  $20^\circ$  and  $30^\circ$  at  $1435~\text{cm}^{-1}$  and  $1375~\text{cm}^{-1}$  respectively. (d) In the Fourier space, the transition of TBLG system from commensurate lattice  $(10^\circ)$  to incommensurate lattice  $(20^\circ$  and  $30^\circ)$  is shown. The rotational symmetry is near 6-fold for  $10^\circ$  gradually reaching 12-fold for  $30^\circ$  which is also a quasi-crystalline state.

# Acknowledgement

The authors acknowledge the funding from SERB Startup Research Grant and DST Nanomission, India. VK, NG and AR acknowledge funding from AOARD (Asian Office of Aerospace Research and Development) under Grant No. FA2386-21-1-4014.VK, VP, AMB and SP acknowledge the STEP facility at IIT Kharagpur. SM, NM, and AKS thank the Materials Research Centre (MRC), Supercomputer Education and Research Centre (SERC), and Solid State and Structural Chemistry Unit (SSCU), Indian Institute of Science, Bangalore, for providing the required computational facilities. SM, NM, and AKS also acknowledge support from The Institute of Eminence (IoE) scheme of The Ministry of Human Resource Development, Government of India. K.W. and T.T. acknowledge support from the JSPS KAKENHI (Grant Numbers 21H05233 and 23H02052) and World Premier International Research Center Initiative (WPI), MEXT, Japan.

# References

- (1) Cao, Y.; Fatemi, V.; Fang, S.; Watanabe, K.; Taniguchi, T.; Kaxiras, E.; Jarillo-Herrero, P. Unconventional superconductivity in magic-angle graphene superlattices. *Nature* **2018**, *556*, 43–50.
- (2) Cao, Y.; Fatemi, V.; Demir, A.; Fang, S.; Tomarken, S. L.; Luo, J. Y.; Sanchez-Yamagishi, J. D.; Watanabe, K.; Taniguchi, T.; Kaxiras, E.; Ashoori, R. C.; Jarillo-Herrero, P. Correlated insulator behaviour at half-filling in magic-angle graphene superlattices. *Nature* **2018**, *556*, 80–84.
- (3) Sharpe, A. L.; Fox, E. J.; Barnard, A. W.; Finney, J.; Watanabe, K.; Taniguchi, T.; Kastner, M. A.; Goldhaber-Gordon, D. Emergent ferromagnetism near three-quarters filling in twisted bilayer graphene. *Science* **2019**, *365*, 605–608.
- (4) Serlin, M.; Tschirhart, C. L.; Polshyn, H.; Zhang, Y.; Zhu, J.; Watanabe, K.; Taniguchi, T.;

- Balents, L.; Young, A. F. Intrinsic quantized anomalous Hall effect in a moiré heterostructure. *Science* **2020**, *367*, 900–903.
- (5) Bistritzer, R.; MacDonald, A. H. Moiré bands in twisted double-layer graphene. *Proceedings* of the National Academy of Sciences **2011**, 108, 12233–12237.
- (6) Yoo, H. et al. Atomic and electronic reconstruction at the van der Waals interface in twisted bilayer graphene. *Nature Materials* **2019**, *18*, 448–453.
- (7) Ahn, S. J.; Moon, P.; Kim, T.-H.; Kim, H.-W.; Shin, H.-C.; Kim, E. H.; Cha, H. W.; Kahng, S.-J.; Kim, P.; Koshino, M.; Son, Y.-W.; Yang, C.-W.; Ahn, J. R. Dirac electrons in a dodecagonal graphene quasicrystal. *Science* **2018**, *361*, 782–786.
- (8) Yao, W.; Wang, E.; Bao, C.; Zhang, Y.; Zhang, K.; Bao, K.; Chan, C. K.; Chen, C.; Avila, J.; Asensio, M. C.; Zhu, J.; Zhou, S. Quasicrystalline 30° twisted bilayer graphene as an incommensurate superlattice with strong interlayer coupling. *Proceedings of the National Academy of Sciences* **2018**, *115*, 6928–6933.
- (9) Pezzini, S.; Mišeikis, V.; Piccinini, G.; Forti, S.; Pace, S.; Engelke, R.; Rossella, F.; Watanabe, K.; Taniguchi, T.; Kim, P.; Coletti, C. 30°-Twisted Bilayer Graphene Quasicrystals from Chemical Vapor Deposition. *Nano Letters* **2020**, *20*, 3313–3319.
- (10) Utama, M. I. B. et al. Visualization of the flat electronic band in twisted bilayer graphene near the magic angle twist. *Nature Physics* **2021**, *17*, 184–188.
- (11) Jiang, Y.; Lai, X.; Watanabe, K.; Taniguchi, T.; Haule, K.; Mao, J.; Andrei, E. Y. Charge order and broken rotational symmetry in magic-angle twisted bilayer graphene. *Nature* **2019**, *573*, 91–95.
- (12) Kerelsky, A.; McGilly, L. J.; Kennes, D. M.; Xian, L.; Yankowitz, M.; Chen, S.; Watanabe, K.; Taniguchi, T.; Hone, J.; Dean, C.; Rubio, A.; Pasupathy, A. N. Maximized electron interactions at the magic angle in twisted bilayer graphene. *Nature* **2019**, *572*, 95–100.

- (13) Choi, Y.; Kemmer, J.; Peng, Y.; Thomson, A.; Arora, H.; Polski, R.; Zhang, Y.; Ren, H.; Alicea, J.; Refael, G.; von Oppen, F.; Watanabe, K.; Taniguchi, T.; Nadj-Perge, S. Electronic correlations in twisted bilayer graphene near the magic angle. *Nature Physics* **2019**, *15*, 1174–1180.
- (14) Xie, Y.; Lian, B.; Jäck, B.; Liu, X.; Chiu, C.-L.; Watanabe, K.; Taniguchi, T.; Bernevig, B. A.; Yazdani, A. Spectroscopic signatures of many-body correlations in magic-angle twisted bilayer graphene. *Nature* **2019**, *572*, 101–105.
- (15) Wong, D.; Nuckolls, K. P.; Oh, M.; Lian, B.; Xie, Y.; Jeon, S.; Watanabe, K.; Taniguchi, T.; Bernevig, B. A.; Yazdani, A. Cascade of electronic transitions in magic-angle twisted bilayer graphene. *Nature* **2020**, *582*, 198–202.
- (16) Zondiner, U.; Rozen, A.; Rodan-Legrain, D.; Cao, Y.; Queiroz, R.; Taniguchi, T.; Watan-abe, K.; Oreg, Y.; von Oppen, F.; Stern, A.; Berg, E.; Jarillo-Herrero, P.; Ilani, S. Cascade of phase transitions and Dirac revivals in magic-angle graphene. *Nature* **2020**, *582*, 203–208.
- (17) Choi, Y.; Kim, H.; Peng, Y.; Thomson, A.; Lewandowski, C.; Polski, R.; Zhang, Y.; Arora, H. S.; Watanabe, K.; Taniguchi, T.; Alicea, J.; Nadj-Perge, S. Correlation-driven topological phases in magic-angle twisted bilayer graphene. *Nature* **2021**, *589*, 536–541.
- (18) Nuckolls, K. P.; Oh, M.; Wong, D.; Lian, B.; Watanabe, K.; Taniguchi, T.; Bernevig, B. A.; Yazdani, A. Strongly correlated Chern insulators in magic-angle twisted bilayer graphene.

  Nature 2020, 588, 610–615.
- (19) Lisi, S. et al. Observation of flat bands in twisted bilayer graphene. *Nature Physics* **2021**, *17*, 189–193.
- (20) Sato, K.; Hayashi, N.; Ito, T.; Masago, N.; Takamura, M.; Morimoto, M.; Maekawa, T.; Lee, D.; Qiao, K.; Kim, J.; Nakagahara, K.; Wakabayashi, K.; Hibino, H.; Norimatsu, W. Observation of a flat band and bandgap in millimeter-scale twisted bilayer graphene. *Communications Materials* **2021**, *2*, 117.

- (21) Ferrari, A. C.; Meyer, J. C.; Scardaci, V.; Casiraghi, C.; Lazzeri, M.; Mauri, F.; Piscanec, S.; Jiang, D.; Novoselov, K. S.; Roth, S.; Geim, A. K. Raman Spectrum of Graphene and Graphene Layers. *Physical Review Letters* **2006**, *97*, 187401.
- (22) Ferrari, A. C. Raman spectroscopy of graphene and graphite: Disorder, electron–phonon coupling, doping and nonadiabatic effects. *Solid State Communications* **2007**, *143*, 47–57.
- (23) Eckmann, A.; Felten, A.; Mishchenko, A.; Britnell, L.; Krupke, R.; Novoselov, K. S.; Casiraghi, C. Probing the Nature of Defects in Graphene by Raman Spectroscopy. *Nano Letters* **2012**, *12*, 3925–3930.
- (24) Lui, C. H.; Li, Z.; Chen, Z.; Klimov, P. V.; Brus, L. E.; Heinz, T. F. Imaging Stacking Order in Few-Layer Graphene. *Nano Letters* **2011**, *11*, 164–169.
- (25) Poncharal, P.; Ayari, A.; Michel, T.; Sauvajol, J.-L. Raman spectra of misoriented bilayer graphene. *Physical Review B* **2008**, *78*, 113407.
- (26) Cong, C.; Yu, T.; Sato, K.; Shang, J.; Saito, R.; Dresselhaus, G. F.; Dresselhaus, M. S. Raman Characterization of ABA- and ABC-Stacked Trilayer Graphene. *ACS Nano* **2011**, *5*, 8760–8768.
- (27) Podila, R.; Rao, R.; Tsuchikawa, R.; Ishigami, M.; Rao, A. M. Raman Spectroscopy of Folded and Scrolled Graphene. *ACS Nano* **2012**, *6*, 5784–5790.
- (28) Gupta, A. K.; Tang, Y.; Crespi, V. H.; Eklund, P. C. Nondispersive Raman D band activated by well-ordered interlayer interactions in rotationally stacked bilayer graphene. *Physical Review B* **2010**, 82, 241406.
- (29) Carozo, V.; Almeida, C. M.; Ferreira, E. H. M.; Cançado, L. G.; Achete, C. A.; Jorio, A. Raman Signature of Graphene Superlattices. *Nano Letters* **2011**, *11*, 4527–4534.
- (30) Ramnani, P.; Neupane, M. R.; Ge, S.; Balandin, A. A.; Lake, R. K.; Mulchandani, A. Raman spectra of twisted CVD bilayer graphene. *Carbon* **2017**, *123*, 302–306.

- (31) Lu, C.-C.; Lin, Y.-C.; Liu, Z.; Yeh, C.-H.; Suenaga, K.; Chiu, P.-W. Twisting Bilayer Graphene Superlattices. *ACS Nano* **2013**, *7*, 2587–2594.
- (32) Zhou, W.-G.; Leng, Y.-C.; Liu, L.-X.; Yang, M.-M.; Liu, W.; Liu, J.-L.; Zhao, P.; Liu, Y.; Wang, L.-L.; Shang, Y.-X.; Li, X.-L.; Zhao, X.-H.; Liu, X.-L.; Xu, Y. Twist angle dependent absorption feature induced by interlayer rotations in CVD bilayer graphene. *Nanophotonics* **2021**, *10*, 2695–2703.
- (33) He, R.; Chung, T.-F.; Delaney, C.; Keiser, C.; Jauregui, L. A.; Shand, P. M.; Chancey, C. C.; Wang, Y.; Bao, J.; Chen, Y. P. Observation of Low Energy Raman Modes in Twisted Bilayer Graphene. *Nano Letters* **2013**, *13*, 3594–3601.
- (34) Moutinho, M. V. O.; Venezuela, P.; Pimenta, M. A. Raman Spectroscopy of Twisted Bilayer Graphene. *C* **2021**, *7*, 10.
- (35) Xu, B.; Hao, H.; Huang, J.; Zhao, Y.; Yang, T.; Zhang, J.; Tong, L. Twist-Induced New Phonon Scattering Pathways in Bilayer Graphene Probed by Helicity-Resolved Raman Spectroscopy. *The Journal of Physical Chemistry C* 2022, 126, 10487–10493.
- (36) Yeh, C.-H.; Lin, Y.-C.; Nayak, P. K.; Lu, C.-C.; Liu, Z.; Suenaga, K.; Chiu, P.-W. Probing interlayer coupling in twisted single-crystal bilayer graphene by Raman spectroscopy. *Journal of Raman Spectroscopy* **2014**, *45*, 912–917.
- (37) Cong, C.; Yu, T. Evolution of Raman G and G' (2D) modes in folded graphene layers. *Physical Review B* **2014**, *89*, 235430.
- (38) Havener, R. W.; Zhuang, H.; Brown, L.; Hennig, R. G.; Park, J. Angle-Resolved Raman Imaging of Interlayer Rotations and Interactions in Twisted Bilayer Graphene. *Nano Letters* 2012, 12, 3162–3167.
- (39) Kim, K.; Coh, S.; Tan, L. Z.; Regan, W.; Yuk, J. M.; Chatterjee, E.; Crommie, M. F.; Cohen, M. L.; Louie, S. G.; Zettl, A. Raman Spectroscopy Study of Rotated Double-Layer

- Graphene: Misorientation-Angle Dependence of Electronic Structure. *Physical Review Letters* **2012**, *108*, 246103.
- (40) Ni, Z.; Wang, Y.; Yu, T.; You, Y.; Shen, Z. Reduction of Fermi velocity in folded graphene observed by resonance Raman spectroscopy. *Physical Review B* **2008**, *77*, 235403.
- (41) Wang, Y. et al. Resonance Raman spectroscopy of G-line and folded phonons in twisted bilayer graphene with large rotation angles. *Applied Physics Letters* **2013**, *103*, 123101.
- (42) Moutinho, M. V. O.; Eliel, G. S. N.; Righi, A.; Gontijo, R. N.; Paillet, M.; Michel, T.; Chiu, P.-W.; Venezuela, P.; Pimenta, M. A. Resonance Raman enhancement by the intralayer and interlayer electron–phonon processes in twisted bilayer graphene. *Scientific Reports* 2021, 11, 17206.
- (43) Eliel, G. S. N.; Moutinho, M. V. O.; Gadelha, A. C.; Righi, A.; Campos, L. C.; Ribeiro, H. B.; Chiu, P.-W.; Watanabe, K.; Taniguchi, T.; Puech, P.; Paillet, M.; Michel, T.; Venezuela, P.; Pimenta, M. A. Intralayer and interlayer electron–phonon interactions in twisted graphene heterostructures. *Nature Communications* 2018, 9, 1221.
- (44) Campos-Delgado, J.; Cançado, L. G.; Achete, C. A.; Jorio, A.; Raskin, J.-P. Raman scattering study of the phonon dispersion in twisted bilayer graphene. *Nano Research* **2013**, *6*, 269–274.
- (45) Huang, S.; Yankowitz, M.; Chattrakun, K.; Sandhu, A.; LeRoy, B. J. Evolution of the electronic band structure of twisted bilayer graphene upon doping. *Scientific Reports* **2017**, *7*, 7611.
- (46) Schäpers, A.; Sonntag, J.; Valerius, L.; Pestka, B.; Strasdas, J.; Watanabe, K.; Taniguchi, T.; Wirtz, L.; Morgenstern, M.; Beschoten, B.; Dolleman, R. J.; Stampfer, C. Raman imaging of twist angle variations in twisted bilayer graphene at intermediate angles. 2D Materials 2022, 9, 045009.

- (47) Zhang, X.; Zhang, R.; Wang, Y.; Zhang, Y.; Jiang, T.; Deng, C.; Zhang, X.; Qin, S. Inplane anisotropy in twisted bilayer graphene probed by Raman spectroscopy. *Nanotechnology* **2019**, *30*, 435702.
- (48) Barbosa, T. C.; Gadelha, A. C.; Ohlberg, D. A. A.; Watanabe, K.; Taniguchi, T.; Medeiros-Ribeiro, G.; Jorio, A.; Campos, L. C. Raman spectra of twisted bilayer graphene close to the magic angle. *2D Materials* **2022**, *9*, 025007.
- (49) Pizzocchero, F.; Gammelgaard, L.; Jessen, B. S.; Caridad, J. M.; Wang, L.; Hone, J.; Bøggild, P.; Booth, T. J. The hot pick-up technique for batch assembly of van der Waals heterostructures. *Nature Communications* **2016**, *7*, 11894.
- (50) Hicks, J.; Sprinkle, M.; Shepperd, K.; Wang, F.; Tejeda, A.; Taleb-Ibrahimi, A.; Bertran, F.; Fèvre, P. L.; de Heer, W. A.; Berger, C.; Conrad, E. H. Symmetry breaking in commensurate graphene rotational stacking: Comparison of theory and experiment. *Physical Review B* 2011, 83, 205403.
- (51) Uchida, K.; Furuya, S.; Iwata, J.-I.; Oshiyama, A. Atomic corrugation and electron localization due to Moiré patterns in twisted bilayer graphenes. *Physical Review B* **2014**, *90*, 155451.
- (52) Luican, A.; Li, G.; Reina, A.; Kong, J.; Nair, R. R.; Novoselov, K. S.; Geim, A. K.; Andrei, E. Y. Single-Layer Behavior and Its Breakdown in Twisted Graphene Layers. *Physical Review Letters* 2011, 106, 126802.
- (53) Malard, L.; Pimenta, M.; Dresselhaus, G.; Dresselhaus, M. Raman spectroscopy in graphene. *Physics Reports* **2009**, *473*, 51–87.
- (54) Kresse, G.; Furthmüller, J. Efficiency of ab-initio total energy calculations for metals and semiconductors using a plane-wave basis set. *Computational Materials Science* **1996**, *6*, 15–50.

- (55) Kresse, G.; Furthmüller, J. Efficient iterative schemes for ab initio total-energy calculations using a plane-wave basis set. *Physical Review B* **1996**, *54*, 11169–11186.
- (56) NE, M. L. O.; Boujnah, M.; Benyoussef, A.; Kenz, A. E. Electronic and Electrical Conductivity of AB and AA-Stacked Bilayer Graphene with Tunable Layer Separation. *Journal of Superconductivity and Novel Magnetism* 2017, 30, 1263–1267.
- (57) Popov, V. N. Raman bands of twisted bilayer graphene. *Journal of Raman Spectroscopy* **2018**, 49, 31–35.
- (58) Brihuega, I.; Mallet, P.; González-Herrero, H.; de Laissardière, G. T.; Ugeda, M. M.; Magaud, L.; Gómez-Rodríguez, J. M.; Ynduráin, F.; Veuillen, J.-Y. Unraveling the Intrinsic and Robust Nature of van Hove Singularities in Twisted Bilayer Graphene by Scanning Tunneling Microscopy and Theoretical Analysis. *Physical Review Letters* 2012, 109, 196802.
- (59) Popov, V. N. Two-phonon Raman bands of bilayer graphene: Revisited. *Carbon* **2015**, *91*, 436–444.
- (60) Samsonidze, G. G.; Saito, R.; Jorio, A.; Filho, A. G. S.; Grüneis, A.; Pimenta, M. A.; Dresselhaus, G.; Dresselhaus, M. S. Phonon Trigonal Warping Effect in Graphite and Carbon Nanotubes. *Physical Review Letters* **2003**, *90*, 027403.
- (61) Jorio, A.; Saito, R.; Hafner, J. H.; Lieber, C. M.; Hunter, M.; McClure, T.; Dresselhaus, G.; Dresselhaus, M. S. Structural (n,m) Determination of Isolated Single-Wall Carbon Nanotubes by Resonant Raman Scattering. *Physical Review Letters* 2001, 86, 1118–1121.
- (62) Cong, C.; Yu, T.; Saito, R.; Dresselhaus, G. F.; Dresselhaus, M. S. Second-Order Overtone and Combination Raman Modes of Graphene Layers in the Range of 1690 2150 cm<sup>-1</sup>. *ACS Nano* **2011**, *5*, 1600–1605.
- (63) Rao, R.; Podila, R.; Tsuchikawa, R.; Katoch, J.; Tishler, D.; Rao, A. M.; Ishigami, M. Effects

- of Layer Stacking on the Combination Raman Modes in Graphene. *ACS Nano* **2011**, *5*, 1594–1599.
- (64) Woods, C. R. et al. Commensurate–incommensurate transition in graphene on hexagonal boron nitride. *Nature Physics* **2014**, *10*, 451–456.
- (65) Kresse, G.; Joubert, D. From ultrasoft pseudopotentials to the projector augmented-wave method. *Physical Review B* **1999**, *59*, 1758–1775.
- (66) Blöchl, P. E. Projector augmented-wave method. *Physical Review B* **1994**, *50*, 17953–17979.
- (67) Perdew, J. P.; Burke, K.; Ernzerhof, M. Generalized Gradient Approximation Made Simple. *Physical Review Letters* **1996**, *77*, 3865–3868.
- (68) Grimme, S. Semiempirical GGA-type density functional constructed with a long-range dispersion correction. *Journal of Computational Chemistry* **2006**, 27, 1787–1799.
- (69) Monkhorst, H. J.; Pack, J. D. Special points for Brillouin-zone integrations. *Physical Review B* **1976**, *13*, 5188–5192.